Appl. Math. Mech. -Engl. Ed., **46**(10), 1867–1882 (2025)

APPLIED MATHEMATICS AND MECHANICS (ENGLISH EDITION)

https://doi.org/10.1007/s10483-025-3304-7

Vibration and response behaviors of composite sandwich cylindrical shells with a carbon nanotube-reinforced damping gel honeycomb core*

Peiyao XU[1,2], Zhuo XU[3], Shang GENG[1,2], Hui LI[1,2,†], Yan ZHOU[4], Haijun WANG[5], Jian XIONG[6], Zeng LIN[1,2], Jun LI[7]

1. School of Mechanical Engineering and Automation, Northeastern University, Shenyang 110819, China;
2. Key Laboratory of Vibration and Control of Aero-Propulsion Systems, Ministry of Education of China, Northeastern University, Shenyang 110819, China;
3. School of Mechanical Engineering, Northeast Electric Power University, Jilin 132014, Jilin Province, China;
4. Jilin General Aviation Vocational and Technical College, Jilin 132014, Jilin Province, China;
5. School of Aeronautics, Shanghai Dianji University, Shanghai 201306, China;
6. Center for Composite Materials and Structures, Harbin Institute of Technology, Harbin 150001, China;
7. Jiangsu Xinyang New Materials Co., Ltd., Yangzhou 225100, Jiangsu Province, China

(Received Jul. 1, 2025 / Revised Aug. 20, 2025)

Abstract This study provides a thorough investigation into the vibration behavior and impulse response characteristics of composite honeycomb cylindrical shells filled with damping gel (DG-FHCSs). To address the limitations of existing methods, a dynamic model is developed for both free and forced vibration scenarios. These models incorporate the virtual spring technology to accurately simulate a wide range of boundary conditions. Using the first-order shear deformation theory in conjunction with the Jacobi orthogonal polynomials, an energy expression is formulated, and the natural frequencies and mode shapes are determined via the Ritz method. Based on the Newmark-β method, the pulse response amplitudes and attenuation characteristics under various transient excitation loads are analyzed and evaluated. The accuracy of the theoretical model and the vibration suppression capability of the damping gel are experimentally validated. Furthermore, the effects of key structural parameters on the natural frequency and vibration response are systematically examined.

* Citation: XU, P. Y., XU, Z., GENG, S., LI, H., ZHOU, Y., WANG, H. J., XIONG, J., LIN, Z., and LI, J. Vibration and response behaviors of composite sandwich cylindrical shells with a carbon nanotube-reinforced damping gel honeycomb core. *Applied Mathematics and Mechanics* (*English Edition*), **46**(10), 1867–1882 (2025) https://doi.org/10.1007/s10483-025-3304-7

† Corresponding author, E-mail: lh200300206@163.com

Project supported by the National Natural Science Foundation of China (Nos. 12472005 and 52175079), the Aerospace Science Foundation of China (No. 2022Z009050002), the Key Laboratory of Vibration and Control of Aero-Propulsion System, Ministry of Education of China (No. VCAME201603), and the Tai-Hang Laboratory Program (No. AK023)

Key words dynamic model, honeycomb sandwich shell, damping gel, anti-vibration, transient response

Chinese Library Classification O326, O328
2010 Mathematics Subject Classification 74H45, 74E30

1 Introduction

The sandwich structure is a composite structure consisting of two face panels (referred to as the "skin" layers) and a lightweight core material layer (referred to as the "core" layer). This design aims to reduce weight while maintaining or even enhancing the overall strength and stiffness of the structure. Additionally, it improves other properties such as thermal insulation, acoustic insulation, and fatigue resistance[1]. Fiber-reinforced composite honeycomb sandwich cylindrical shells (FHCSs) have gained extensive applications across various fields owing to their superior lightweight design and exceptional mechanical properties. For example, the protective structures of aviation equipment contain a significant number of honeycomb sandwich shell components[2–5]. Figure 1(a) shows the fiber-reinforced honeycomb cylindrical shell in the aerospace industry. Figure 1(b) shows actual cylindrical prototypes of the upper and lower interstage structures for the second stage of Russian launcher Proton-M[6]. Figure 1(c) shows all composite honeycomb grid-stiffened fuselage utilized for the Russian civil aircraft[7]. This type of sandwich shell is typically subjected to severe dynamic loads, including air inflow, bird strikes, and hydraulic pump pulsations. These loads can induce excessive vibration responses, potentially leading to fractures and fatigue damage[8–11]. Therefore, it is crucial to conduct a comprehensive analysis of the free vibration characteristics and transient dynamic response behaviors of the structure. Furthermore, the filling method represents an economical and effective approach to enhance the stiffness, strength, vibration resistance, and energy absorption performance of honeycomb sandwich structures[12–15]. Consequently, this technique has garnered significant attention in recent years. Thus, developing a high-performance damping gel material capable of effectively suppressing vibration and absorbing impact energy, and comprehensively analyzing the dynamic characteristics of structures, are crucial for enhancing the reliability and durability of honeycomb sandwich structures[16–18].

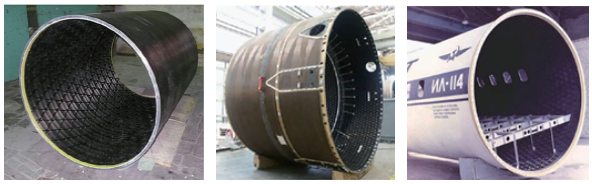

(a) (b) (c)

Fig. 1 Example applications of composite honeycomb grid-stiffened shells: (a) fiber-reinforced honeycomb sandwich shells in the aerospace industry; (b) all CFRP composite stiffened interstage for the second stage of Russian launcher Proton-M[6]; (c) all composite grid-stiffened fuselage utilized for the Russian civil aircraft[7] (color online)

In recent years, the dynamic characteristics of sandwich cylindrical shells with various core layers have emerged as a research hotspot. For instance, Liu and Sun[19] employed a combination of theoretical modeling and experimental validation to investigate the free vibration behavior of carbon fiber-reinforced cylindrical origami sandwich structures (CFSSs). Yadav et al.[20] investigated the nonlinear dynamic behavior of cylindrical sandwich shells featuring porous core materials and carbon nanotube-reinforced panels. The study further examined the effects of the porosity coefficient, the thickness ratio of the core material to the panel, and the boundary conditions on their deformation characteristics. Van Quyen et al.[21] investigated

the nonlinear free and forced vibration behaviors of sandwich cylindrical panels with carbon nanotube-reinforced composite faces. Li et al.[22] investigated the vibration characteristics of fiber-reinforced composite hexagonal honeycomb sandwich cylindrical-spherical combined shells (HHC-FRCS-CS). The study analyzed the influence of geometric parameters on the dynamic performance of the structure and concluded that vibration suppression can be significantly enhanced by reducing the ratios of the HHC-FRCS-CS thickness to the total thickness and the honeycomb unit wall thickness to the overall radius, while increasing both ratios of the honeycomb unit length to the overall radius and the characteristic angle of the HHC-FRCS-CS. Shahali et al.[23] utilized the semi-analytical method, which combines trigonometric function expansion with the generalized differential quadrature method, to investigate the vibration and damping characteristics of cylindrical sandwich shells featuring functionally-graded material panels and an electro-rheological core. Keleshteri and Jelovica[24] conducted an analysis of the vibration and buckling behaviors of cylindrical sandwich plates with an improved functionally-graded metal foam core. Liu et al.[25] focused on analyzing the vibration characteristics of corrugated cylindrical shells and systematically investigated the effects of various parameters, including the period, radius, height of corrugated, units, and different boundary conditions, on the vibration behavior of corrugated shells. Li et al.[26] developed a vibration suppression performance model for composite pyramid truss sandwich cylindrical shell plates. Through experimental validation, the study analyzed the effects of key parameters, such as the composite ply angle, the damping coating thickness ratio and modulus ratio, the pyramid truss core thickness ratio and modulus ratio, and their corresponding vibration characteristics. Karimiasl and Alibeigloo[27] investigated the free and forced vibrations of sandwich cylindrical plates featuring auxetic cores under hygrothermal conditions. Heidari-Soureshjani et al.[28] investigated the vibration characteristics of honeycomb cylindrical shells with rectangular openings. The study systematically examined the effects of opening characteristics (opening angle, position, and geometric shape), sandwich structure properties (core layer thickness ratio, inclination angle, and auxetic parameter), and boundary conditions on the vibration behavior. The accuracy of the proposed model was validated through experimental comparisons. Jian et al.[29] investigated the vibration characteristics of a fiber-reinforced composite sandwich cylindrical shell. This shell features a functionally-graded graphene-reinforced porous composite core layer and is subjected to discontinuous boundary conditions. Wu et al.[30] analyzed the vibration characteristics of the sandwich cylindrical shell with a metal rubber core in a thermal environment. Dong et al.[31] analyzed the vibration and response behavior of sandwich cylindrical shells with corrugated-honeycomb mixed cores and functionally-graded composite skins under a non-uniform thermal environment. Thang et al.[32] utilized the refined trigonometric shear deformation theory (RTSDT) to investigate the free vibration characteristics of honeycomb sandwich cylindrical shells reinforced with graphene nanoplatelets/polymer (GNP) coatings. The effects of axial and circumferential wave numbers, geometric parameters, material properties, and elastic foundation parameters on the vibration frequency were systematically analyzed. Yavari and Alibeigloo[33] analyzed the free vibration and buckling behaviors of sandwich cylindrical shells with auxetic honeycomb cores and shape memory alloy wire-reinforced panels using the differential quadrature method. Dong et al.[34] analyzed the vibration behavior of sandwich cylindrical shells with corrugated honeycomb cores and three-phase composite panels under thermal conditions. The study explored the frequencies and various harmonic resonance behaviors under different configuration schemes and thermal effects, ultimately providing practical guidelines for enhancing the dynamic performance of the structure. Ni et al.[35] proposed a prediction model for honeycomb sandwich cylindrical shell with dual deformation modes. The circumferential band vibration characteristics were analyzed through quasi-static compression experiments and dynamic modeling. Yadav[36] investigated the free and forced vibration behaviors of the sandwich cylindrical shells featuring auxetic honeycomb cores and carbon nanotube-reinforced face panels. Qin et al.[37] systematically developed a free vibration analysis model

for rotating functionally-graded carbon nanotube-reinforced composite cylindrical shells. Based on the first-order shear deformation theory (FSDT) and Donnell shell theory, the authors introduced an artificial spring technique to simulate various boundary conditions, and applied the Chebyshev-Ritz method to effectively capture the coupling effects of the Coriolis force and centrifugal force induced by rotation. The study elucidated how the distribution pattern and volume fraction of carbon nanotubes, boundary stiffness, and geometric parameters influence the traveling wave vibration characteristics, thereby offering a solid theoretical foundation for the dynamic design of rotating shell structures. Zhu et al.[38] proposed a localized constrained layer damping modeling and topology optimization approach applicable to cylindrical shells with general boundary conditions. A three-layer coupled dynamic model was developed using the Rayleigh-Ritz method, and evolutionary structural optimization was employed to determine the optimal distribution of damping materials.

In recent years, remarkable advancements have been achieved in the development of gel materials, particularly in the field of damping applications. By employing innovative molecular mechanisms and sophisticated material designs, researchers have successfully developed novel gel materials with superior damping capabilities[39]. For instance, Zhang et al.[40] fabricated oxidized sodium alginate/polyacrylamide double-network hydrogels and systematically investigated their viscoelastic properties and damping performances. The results demonstrated that when the methylene dimethyl amide concentration was set at 0.02%, the damping factor of the hydrogel remained above 0.3 across a temperature range of 0 °C–125 °C, thereby exhibiting exceptional damping characteristics. Deastra et al.[41] utilized the shaking table experimental method to evaluate the vibration control performance of gel-based dampers in a three-story steel structure and further analyzed the effects of viscous damping and hysteretic damping mechanisms on the multiple resonance peak behaviors of the structure. Koruk and Rajagopal[42] performed a comprehensive theoretical investigation into the viscoelastic parameters and damping properties of engineering materials, with particular emphasis on soft material systems. This study provided a valuable framework for characterizing the damping properties of gel-based damping materials. Through microphase separation analysis, Zhang et al.[43] revealed that dielectric gel structures exhibit exceptional vibration damping across a wide frequency range while maintaining excellent optical transparency — a unique combination that makes them promising for demanding flexible sensor applications. Ding et al.[44] fabricated synthetic polydimethylsiloxane-based composite gels and assessed their damping performance using the low-speed impact method. Additionally, they evaluated the damping attenuation characteristics of these gels across various temperature ranges.

Existing studies on honeycomb sandwich structures have predominantly concentrated on harmonic vibration characteristics, with the transient dynamic behavior receiving disproportionately limited research attention. Furthermore, the majority of studies have neglected the significant potential benefits of gel damping materials in reducing vibrations and enhancing resistance to transient responses. Aiming to address the scarcity of studies on the modeling and analysis of free vibration and transient dynamics of honeycomb sandwich structures with damping gel materials, this paper focuses on the DG-FHCS as the research object. An analytical model for the DG-FHCS is established to comprehensively investigate its free vibration characteristics and transient response behavior.

First, the analytical models of the DG-FHCS under four types of transient excitation waves are developed, and the solution principle is elaborated in Section 2. Section 3 conducts a detailed convergence analysis of the relevant parameters in the model and compares the results with those obtained from finite element software to validate the accuracy of the model. Then, in Section 4, the FHCS and DG-FHCS are fabricated. The accuracy of the model is validated, and the vibration reduction performance of the damping gel is evaluated through experimental comparisons. In Section 5, the influence of relevant parameters on the vibration characteristics of the structure is analyzed in detail. Finally, in Section 6, the key research conclusions

are summarized, along with several practical designs and engineering recommendations. The innovation points of this paper are as follows. (i) A silicon-based damping gel material is synthesized. (ii) An advanced model for predicting the vibration characteristics of the DG-FHCS is developed. (iii) The vibration reduction performance of shells with and without damping gel materials is systematically assessed. (iv) Several constructive recommendations for optimizing the structural parameters of the DG-FHCS to enhance its vibration resistance are proposed.

2 Theoretical deduction

The dynamic models of FHCSs and DG-FHCSs are developed, and the free vibration solutions are derived using the first-order shear deformation theory in conjunction with the Jacobi-Ritz method. Additionally, the transient dynamic response solutions are obtained based on the Newmark-β method.

2.1 Model description

Figure 2 illustrates the theoretical model of the structure. Specifically, Fig. 2(a) illustrates the detailed layup method of the sandwich structure. This structure consists of inner and outer fiber skin layers enclosing a honeycomb core filled with damping gel. The thicknesses of the inner skin, honeycomb core, and outer skin are denoted as h^{f1}, h^{o}, and h^{f2}, respectively. Figure 2(b) illustrates the laying method of the fiber skin. The direction of parallel fibers is denoted as 1, while the direction of vertical fibers is denoted as 2. Additionally, the direction perpendicular to the 12-plane is denoted as 3. Figure 2(c) presents the comprehensive model of the structure. The length of the shell is represented as L, and the mid-surface radius of the shell is denoted as R. The primary coordinate system is defined as O-$x\theta z$, while the mid-surface modal coordinate system is specified as o-$u_0v_0w_0$. Additionally, the boundary spring comprises three tensional springs (k_u, k_v, and k_w) and two torsional springs (k_θ and k_φ). Figure 2(d) illustrates the honeycomb sandwich structure, where the wall thickness of the honeycomb is denoted as a, the length of the honeycomb arm is denoted as b, and the honeycomb corner angle is denoted as γ. Figure 2(e) illustrates four types of pulse excitation waveforms, specifically the exponential wave, triangular wave, half-sine wave, and square wave. Among these, the excitation duration extends from t_0 to t_1, and the excitation time of the pulse wave is denoted by τ.

2.2 Material parameter equivalence method

According to the Gibson theory, Young's moduli E_1^{h} and E_2^{h}, shear moduli G_{12}^{h}, G_{13}^{h}, and G_{23}^{h} of the honeycomb core can be expressed as[45]

$$\begin{cases} E_1^{\mathrm{h}} = E_{\mathrm{h}}\Big(\dfrac{a}{b}\Big)^3 \dfrac{\cos\gamma}{(1+\sin\gamma)\sin^2\gamma}\Big(1-\cot^2\gamma\Big(\dfrac{a}{b}\Big)^2\Big), \\ E_2^{\mathrm{h}} = E_{\mathrm{h}}\Big(\dfrac{a}{b}\Big)^3 \dfrac{(1+\sin\gamma)}{\cos^3\gamma}\Big(1-(\sec^2\gamma+\tan^2\gamma)\Big(\dfrac{a}{b}\Big)^2\Big), \end{cases} \tag{1a}$$

$$\begin{cases} G_{12}^{\mathrm{h}} = G_{\mathrm{h}}\Big(\dfrac{a}{b}\Big)^3 \dfrac{(1+\sin\gamma)}{3\cos\gamma}, \quad G_{13}^{\mathrm{h}} = G_{\mathrm{h}}\dfrac{a}{b}\dfrac{\cos\gamma}{(1+\sin\gamma)}, \\ G_{23}^{\mathrm{h}} = \dfrac{1}{2}G_{\mathrm{h}}\dfrac{a}{b}\Big(\dfrac{1+\sin\gamma}{2\cos\gamma}+\dfrac{1+\sin^2\gamma}{2(1+\sin\gamma)\cos\gamma}\Big). \end{cases} \tag{1b}$$

Poisson's ratios ν_{12}^{h} and ν_{21}^{h} of the structure can be expressed as

$$\nu_{12}^{\mathrm{h}} = \frac{\cos^2\gamma}{(1+\sin\gamma)\sin\gamma}\Big(1-\csc^2\gamma\Big(\frac{a}{b}\Big)^2\Big), \quad \nu_{21}^{\mathrm{h}} = \frac{(1+\sin\gamma)\sin\gamma}{\cos^2\gamma}\Big(1-2\sec^2\gamma\Big(\frac{a}{b}\Big)^2\Big). \tag{2}$$

The density ρ^{h} of the structure can be expressed as

$$\rho^{\mathrm{h}} = \rho_{\mathrm{h}}\frac{a}{b}\frac{2}{(1+\sin\gamma)\cos\gamma}, \tag{3}$$

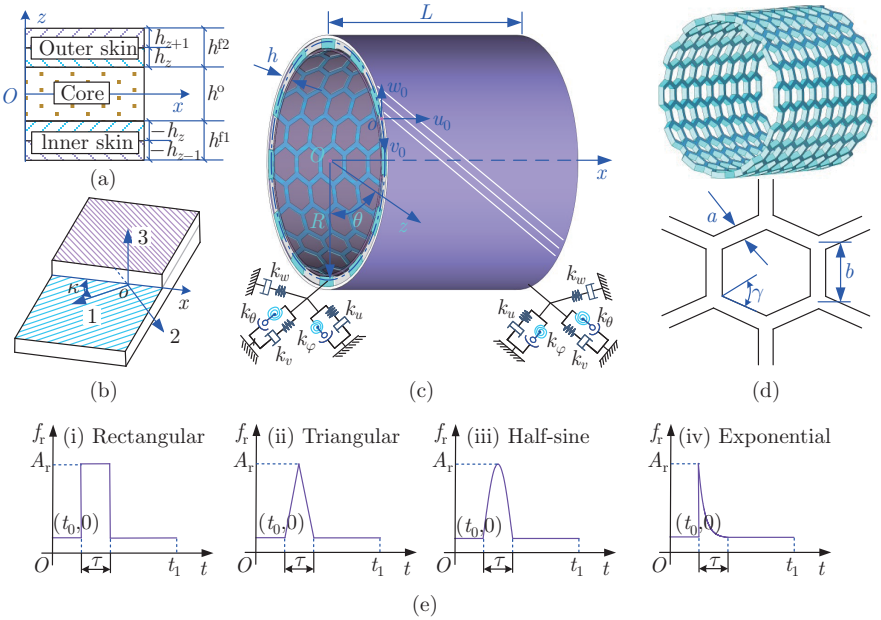

Fig. 2 A theoretical model of DG-FHCS. (a) The ply model of the structure; (b) the layer angle model of fiber-reinforced skin in the local coordinate system o-123; (c) geometric symbols of the overall structure with a cylindrical coordinate system O-$x\theta z$ and boundary springs; (d) geometric parameters of the honeycomb core; (e) schematic representations of (i) exponential, (ii) triangular, (iii) half-sine, and (iv) rectangular pulse excitations (color online)

where the parameters E_{h} and G_{h} represent Young's modulus and the shear modulus of the materials utilized in fabricating honeycomb sandwich structures, respectively, while ρ_{h} denotes the corresponding density.

According to the Hamilton equivalent theory[45], Young's moduli E_1^{o} and E_2^{o}, shear moduli G_{12}^{o}, G_{13}^{o}, and G_{23}^{o} of the damping-filled honeycomb core can be expressed as

$$E_1^{\mathrm{o}} = 1\Big/\Big(\int_0^1 \frac{1}{(E_1^{\mathrm{h}} + |E_{\mathrm{o}} - E_1^{\mathrm{h}}|G_x(\delta))}\mathrm{d}\delta\Big), \quad E_2^{\mathrm{o}} = 1\Big/\Big(\int_0^1 \frac{1}{(E_2^{\mathrm{h}} + |E_{\mathrm{o}} - E_2^{\mathrm{h}}|G_\theta(\delta))}\mathrm{d}\delta\Big), \tag{4a}$$

$$\begin{cases} G_{12}^{\mathrm{o}} = 1\Big/\Big(\int_0^1 \dfrac{1}{(G_{12}^{\mathrm{h}} + |G_{\mathrm{o}} - G_{12}^{\mathrm{h}}|G_z(\delta))}\mathrm{d}\delta\Big), \\ G_{13}^{\mathrm{o}} = 1\Big/\Big(\int_0^1 \dfrac{1}{(G_{13}^{\mathrm{h}} + |G_{\mathrm{o}} - G_{13}^{\mathrm{h}}|G_\theta(\delta))}\mathrm{d}\delta\Big), \\ G_{23}^{\mathrm{o}} = 1\Big/\Big(\int_0^1 \dfrac{1}{(G_{23}^{\mathrm{h}} + |G_{\mathrm{o}} - G_{23}^{\mathrm{h}}|G_x(\delta))}\mathrm{d}\delta\Big). \end{cases} \tag{4b}$$

Poisson's ratios ν_{12}^{o} and ν_{21}^{o} of the damping gel-filled honeycomb core can be expressed as

$$\nu_{12}^{\mathrm{o}} = 1\Big/\Big(\int_0^1 \frac{1}{(\nu_{12}^{\mathrm{h}} + |\nu_{\mathrm{o}} - \nu_{12}^{\mathrm{h}}|G_z(\delta))}\mathrm{d}\delta\Big), \quad \nu_{21}^{\mathrm{o}} = 1\Big/\Big(\int_0^1 \frac{1}{(\nu_{21}^{\mathrm{h}} + |\nu_{\mathrm{o}} - \nu_{21}^{\mathrm{h}}|G_z(\delta))}\mathrm{d}\delta\Big), \tag{5}$$

where the cross-sectional area functions for filling the honeycomb core in the x-, y-, and z-directions are denoted as $G_x(\delta)$, $G_y(\delta)$, and $G_z(\delta)$, respectively. Young's modulus, shear modulus, and Poisson's ratio of the damping gel used for filling are denoted by E_{o}, G_{o}, and ν_{o}, respectively.

In addition, the density of the composite damping-filled honeycomb core is denoted as ρ^{o},

$$\rho^{\mathrm{o}} = \frac{b^2\rho^{\mathrm{h}}\cos\gamma + (2ab\cos\gamma + a^2)\rho_{\mathrm{o}}}{(b\cos\gamma + a)^2}. \tag{6}$$

The stiffness matrix elements of the damping-filled honeycomb core can be denoted as

$$\begin{cases} Q_{11}^{\mathrm{o}} = \dfrac{E_1^{\mathrm{o}}}{(1-\nu_{12}^{\mathrm{o}}\nu_{21}^{\mathrm{o}})}, \quad Q_{12}^{\mathrm{o}} = \dfrac{\nu_{12}^{\mathrm{o}}E_2^{\mathrm{o}}}{(1-\nu_{12}^{\mathrm{o}}\nu_{21}^{\mathrm{o}})}, \\ Q_{21}^{\mathrm{o}} = \dfrac{\nu_{21}^{\mathrm{o}}E_2^{\mathrm{o}}}{(1-\nu_{12}^{\mathrm{o}}\nu_{21}^{\mathrm{o}})}, \quad Q_{22}^{\mathrm{o}} = \dfrac{E_2^{\mathrm{o}}}{(1-\nu_{12}^{\mathrm{o}}\nu_{21}^{\mathrm{o}})}, \\ Q_{66}^{\mathrm{o}} = G_{12}^{\mathrm{o}}, \quad Q_{44}^{\mathrm{o}} = G_{13}^{\mathrm{o}}, \quad Q_{55}^{\mathrm{o}} = G_{23}^{\mathrm{o}}. \end{cases} \tag{7}$$

The elements of the stiffness matrix pertaining to the stretching, coupling, and bending effects in the honeycomb core can be denoted as[47–49]

$$A_{ij}^{\mathrm{o}} = \int_{-\frac{h^{\mathrm{o}}}{2}}^{\frac{h^{\mathrm{o}}}{2}} Q_{ij}^{\mathrm{o}}\mathrm{d}z, \quad B_{ij}^{\mathrm{o}} = \int_{-\frac{h^{\mathrm{o}}}{2}}^{\frac{h^{\mathrm{o}}}{2}} Q_{ij}^{\mathrm{o}}z\mathrm{d}z, \quad D_{ij}^{\mathrm{o}} = \int_{-\frac{h^{\mathrm{o}}}{2}}^{\frac{h^{\mathrm{o}}}{2}} Q_{ij}^{\mathrm{o}}z^2\mathrm{d}z. \tag{8}$$

The stiffness coefficients of the fiber-reinforced skins are presented in the electronic supplementary material[49] (see https://doi.org/10.1007/s10483-025-3304-7).

2.3 Constitutive relation and energy equation

Considering the identical stress-strain relationship between the honeycomb core layer with damping gel and the fiber-reinforced skins, the constitutive relationship of the sandwich cylindrical shell structure incorporates both components. Using the FSDT, the displacement components of the cylindrical shell can be established as follows[50]:

$$U(x,\theta,z,t) = u_0(x,\theta,t) + z\varphi_{xz}^0(x,\theta,t), \tag{9a}$$

$$V(x,\theta,z,t) = v_0(x,\theta,t) + z\varphi_{\theta z}^0(x,\theta,t), \tag{9b}$$

$$W(x,\theta,z,t) = w_0(x,\theta,t), \tag{9c}$$

where the maximum truncation order of the polynomial is denoted by M. The stress and strain relationships at any given position within the structure can be expressed as

$$\varepsilon_x = \varepsilon_x^0 + z\kappa_x^0, \quad \varepsilon_\theta = \varepsilon_\theta^0 + z\kappa_\theta^0, \tag{10a}$$

$$\chi_{x\theta} = \chi_{x\theta} + z\kappa_{x\theta}^0, \quad \chi_{xz} = \chi_{xz}^0, \quad \chi_{\theta z} = \chi_{\theta z}^0, \tag{10b}$$

where the normal strains in the middle surface are denoted as ε_x^0 and ε_θ^0, while the shear strains in the middle surface are represented by $\chi_{x\theta}^0$, χ_{xz}^0, and $\chi_{\theta z}^0$. The curvatures of the middle surface are respectively indicated by κ_x^0, κ_θ^0, and $\kappa_{x\theta}^0$[51],

$$\varepsilon_x^0 = \frac{\partial u_0}{\partial x}, \quad \varepsilon_\theta^0 = \frac{\partial u_0}{R\partial x} + \frac{w_0}{R}, \tag{11a}$$

$$\chi_{x\theta}^0 = \frac{1}{R}\frac{\partial u_0}{\partial\theta} + \frac{\partial v_0}{\partial\phi}, \quad \chi_{xz}^0 = \frac{\partial w_0}{\partial x} + \varphi_{xz}, \quad \chi_{\theta z}^0 = \frac{1}{R}\frac{\partial w_0}{\partial\theta} - \frac{v_0}{R} + \varphi_{\theta z}, \tag{11b}$$

$$\kappa_x^0 = \frac{\partial\varphi_x}{\partial x}, \quad \kappa_\theta^0 = \frac{1}{R}\frac{\partial\varphi_{\theta z}^0}{\partial\theta}, \quad \kappa_{x\theta}^0 = \frac{1}{R}\frac{\partial\varphi_{xz}^0}{\partial\theta} + \frac{\partial\varphi_{\theta z}^0}{\partial x}. \tag{11c}$$

The stress-strain relationship of the structure can be found in the electronic supplementary material. The resultant axial forces (N_x, N_θ, $N_{x\theta}$), bending moments (M_x, M_θ, $M_{x\theta}$), and resultant shear force values (Q_{xz}, $Q_{\theta z}$) can be found in the electronic supplementary material[52].

The structural strain energy can be denoted as

$$\begin{aligned} U_\varepsilon = \frac{1}{2}\int_0^{2\pi}\int_0^L (&N_x\varepsilon_x + N_\theta\varepsilon_\theta + N_{x\theta}\chi_{x\theta} + M_x\kappa_x^0 + M_\theta\kappa_\theta^0 + M_{x\theta}\kappa_{\theta x}^0 \\ &+ Q_{xz}\chi_{xz}^0 + Q_{\theta z}\chi_{\theta z}^0)\mathrm{d}x\mathrm{d}\theta. \end{aligned} \tag{12}$$

The potential energy resulting from the presence of elastic boundaries can be denoted as[53]

$$U_{\mathrm{p}}=\frac{1}{2}\int_0^{2\pi}\int_{-h/2}^{h/2}(k_{u,0}u_0^2+k_{v,0}v_0^2+k_{w,0}w_0^2+k_{\varphi,0}\varphi_{xz}^{02}+k_{\theta,0}\varphi_{\theta z}^{02})_{x=0}\mathrm{d}z\mathrm{d}\theta$$
$$+\frac{1}{2}\int_0^{2\pi}\int_{-h/2}^{h/2}(k_{u,1}u_0^2+k_{v,1}v_0^2+k_{w,1}w_0^2+k_{\varphi,1}\varphi_{xz}^{02}+k_{\theta,1}\varphi_{\theta z}^{02})_{x=L}\mathrm{d}z\mathrm{d}\theta, \tag{13}$$

where $k_{i,0}$ and $k_{i,1}$ $(i=u,v,w,\varphi,\theta)$ represent the values of springs at two sides of the structure.

The kinetic energy T of the structure can be described as follows[53]:

$$T=\frac{1}{2}\int_0^{x}\int_0^{2\pi}\Big(I_1\Big(\Big(\frac{\partial u_0}{\partial t}\Big)^2+\Big(\frac{\partial v_0}{\partial t}\Big)^2+\Big(\frac{\partial w_0}{\partial t}\Big)^2\Big)+2I_2\Big(\Big(\frac{\partial u_0}{\partial t}\Big)\Big(\frac{\partial \varphi_{x0}}{\partial t}\Big)+\Big(\frac{\partial v_0}{\partial t}\Big)\Big(\frac{\partial \varphi_{\theta 0}}{\partial t}\Big)\Big)$$
$$+I_3\Big(\Big(\frac{\partial \varphi_{x0}}{\partial t}\Big)^2+\Big(\frac{\partial \varphi_{\theta 0}}{\partial t}\Big)^2\Big)\Big)R\mathrm{d}\theta\mathrm{d}x, \tag{14}$$

where I_1, I_2, and I_3 represent the inertial components of the DG-FHCSs. The specific expressions are provided in the electronic supplementary material.

2.4 The displacement function and the orthogonal polynomials

Based on Jacobi orthogonal polynomials, the middle surface displacements of the cylindrical shell in the x-, θ-, and z-directions are denoted as u_0, v_0, and w_0, respectively. The torsional deformations of the cylindrical shell in the xz- and θz-planes are denoted as φ_{xz}^0 and $\varphi_{\theta z}^0$, respectively[54–55],

$$u_0=\sum_{\overline{m}=0}^{M}U_mP_{\overline{m}}^{(\alpha,\beta)}(\delta)\cos(n\theta),\quad v_0=\sum_{\overline{m}=0}^{M}V_mP_{\overline{m}}^{(\alpha,\beta)}(\delta)\sin(n\theta), \tag{15a}$$

$$w_0=\sum_{\overline{m}=0}^{M}W_mP_{\overline{m}}^{(\alpha,\beta)}(\delta)\cos(n\theta),\quad \varphi_{xz}^0=\sum_{\overline{m}=0}^{M}\xi_{xm}P_{\overline{m}}^{(\alpha,\beta)}(\delta)\cos(n\theta), \tag{15b}$$

$$\varphi_{\theta z}^0=\sum_{\overline{m}=0}^{M}\xi_{\theta m}P_{\overline{m}}^{(\alpha,\beta)}(\delta)\sin(n\theta), \tag{15c}$$

where the mid-plane modal displacement function of the structure can be expressed as u_0, v_0, w_0, φ_{xz}^0, and $\varphi_{\theta z}^0$. The functions of time and mode shape vectors are expressed as U_m, V_m, W_m, ξ_{xm}, and $\xi_{\theta m}$. The circumferential mode number in the displacement equation is denoted as n. The Jacobi polynomial in the axial direction is denoted as $P_m^{(\alpha,\beta)}(\delta)$[56]. The specific expressions are provided in the electronic supplementary material.

2.5 Free vibration solution and dynamic response solution

The Lagrange function L of the structure can be derived as[57]

$$L=U_{\varepsilon}+U_{\mathrm{p}}-T. \tag{16}$$

Furthermore, using the Rayleigh-Ritz to minimize the partial derivative of L with respect to the coefficients U_m, V_m, W_m, ξ_{xm}, and $\xi_{\theta m}$, the following equation can be obtained:

$$\frac{\partial L}{\partial U_m}=\frac{\partial L}{\partial V_m}=\frac{\partial L}{\partial W_m}=\frac{\partial L}{\partial \xi_{xm}}=\frac{\partial L}{\partial \xi_{\theta m}}=0. \tag{17}$$

Then, the eigenvalue equation can be determined as[58]

$$\boldsymbol{M}\frac{\partial^2\boldsymbol{q}}{\partial t^2}+\boldsymbol{C}\frac{\partial \boldsymbol{q}}{\partial t}+\boldsymbol{K}\boldsymbol{q}=\boldsymbol{F}_t=\boldsymbol{M}\boldsymbol{E}\boldsymbol{x}_g'', \tag{18}$$

where $\boldsymbol{K}$ denotes the stiffness matrix, $\boldsymbol{M}$ denotes the mass matrix, and the specific expression is given in the electronic supplementary material. $\boldsymbol{C}$ denotes the damping matrix. The excitation

force is denoted as $\boldsymbol{F}_t$, and the vibration response displacement of the DG-FHCSs is represented by $\boldsymbol{q}$. The excitation direction indication vector is denoted as

$$\boldsymbol{E} = (\boldsymbol{O}_{m\times t} \ \ \boldsymbol{O}_{m\times t} \ \ \boldsymbol{J}_{m\times t} \ \ \boldsymbol{O}_{m\times t} \ \ \boldsymbol{O}_{m\times t})^{\mathrm{T}}, \tag{19}$$

where the zero matrix and the identity matrix are denoted as $\boldsymbol{O}_{m\times t}$ and $\boldsymbol{J}_{m\times t}$, respectively, both with dimensions $m \times t$, while the basic excitation acceleration is denoted as[59]

$$\boldsymbol{x}_g'' = f_r \overline{k} g. \tag{20}$$

The forms of the four excitation signals are denoted as f_r, and the relationships between their respective signal amplitudes and time are presented in Eqs. (S11)–(S14) of the electronic supplementary material[60]. The magnitude of the acceleration excitation level is denoted by $\overline{k}$, the gravitational acceleration is represented by g, and the time step vector is symbolized as t. The force vector $\boldsymbol{F}_t$ acting on the structure can be constructed by multiplying the mass matrix by the acceleration excitation vector.

Based on the Rayleigh damping model, the damping matrix $\boldsymbol{C}$ of the structure can be found in the electronic supplementary material[61–63].

When both the excitation force vector $\boldsymbol{F}_t$ and the modal damping matrix $\boldsymbol{C}$ are set to zero, Eq. (21) is derived. By solving for its eigenvalue, the natural frequency ω of the structure can be determined,

$$(\boldsymbol{K} - \omega^2 \boldsymbol{M})\boldsymbol{X} = \boldsymbol{0}, \tag{21}$$

where the feature vector is represented as $\boldsymbol{X} = (U_m \ \ V_m \ \ W_m \ \ \xi_{xm} \ \ \xi_{\theta m})^{\mathrm{T}}$. By substituting $\boldsymbol{X}$ into Eq. (15), which describes the mid-plane displacement, the modal shapes of the structure can be accurately determined.

Based on the Newmark-β method, the time-domain response of the structure is solved. The detailed derivation process is provided in the electronic supplementary material.

3 Convergence analysis

In this section, the convergence of the proposed dynamic model is analyzed, and the model is validated through comparison with the finite element software. The results demonstrate that the proposed model exhibits good convergence and shows strong agreement with the simulation results, thereby confirming its validity. The detailed analysis process is provided in the electronic supplementary material.

4 Experimental study

In this section, composite honeycomb sandwich cylindrical shells with filled damping gel and honeycomb sandwich cylindrical shells without damping filling are respectively fabricated, and experimental tests are conducted on the two different cylindrical shells to confirm the effectiveness of the model and the vibration reduction properties of the damping gel.

4.1 Fabrication of the FHCS and DG-FHCS specimens

The detailed preparation process is described in the electronic supplementary material.

4.2 Dynamics experimental system and method

Before the experiment, it is essential to determine the location and number of measurement points on the test specimen, as well as their coordinate positions[64]. To ensure the stability of data acquisition, two acceleration sensors are employed for simultaneous data collection. The primary verification point is the test point 1, while the secondary verification point is the test point 2. Figure 3 gives the location of the pulse excitation point (R, π, $0.8\,L$), the coordinates of measurement point 1 (R, 2π, $0.5\,L$) and point 2 (R, 2π, $0.5\,L$), as well as the modal test

framework models. These details should be established by creating a geometric model of the measurement points using the geometry function module within the LMS test lab software.

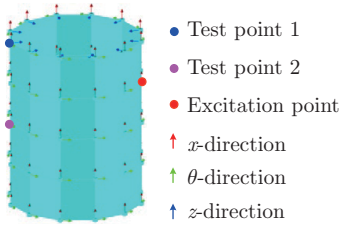

Fig. 3 Test points, excitation point, and modal test framework models (color online)

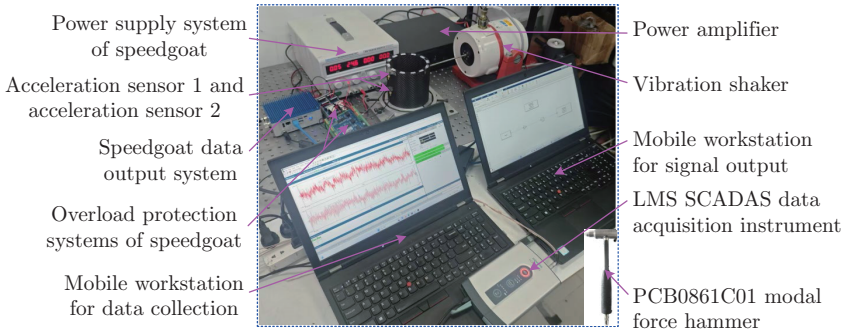

Fig. 4 A test system for measuring the vibration characteristics of the FHCS and DG-FHCS (color online)

Upon completing the preparation process for the FHCS and the DG-FHCS, the experimental test system illustrated in Fig. 4 is established. The established testing system comprises two subsystems, the vibration excitation subsystem and the dynamic signal acquisition subsystem. Among these components, the excitation subsystem consists of a suite of single-point pulse excitation equipment, specifically comprising the vibration shaker, power amplifier, and speedgoat data output system. The transmission of the excitation signal is detailed in the electronic supplementary material. The dynamic signal acquisition subsystem is specifically composed of the LMS SCADAS data acquisition instrument, the PCB 352C33 accelerometer sensor (the sensor exhibits a sensitivity of 100 mV/g (±10%) and operates within a frequency range of 0.5 Hz to 10 kHz. During the test, α-cyanoacrylate adhesive is employed for bonding, with 3M tape used as an auxiliary fixation method) and a computer workstation equipped with LMS Test Lab 2021.1 data processing software. Furthermore, the PCB0861C01 modal force hammer is utilized for conducting modal testing. The sensitivity of the modal force hammer is 11.2 mV/N (±15%), the measurement range is ±440 N, the resonant frequency exceeds 15 kHz, and a medium-hard hammer head is used during the testing process.

Subsequently, modal hammering tests are conducted on specimens both with and without damping gel. Frequency response data from various excitation points are collected. Utilizing the PolyMax technique[65]. A Hamming window function is applied, with a sampling frequency range of 0 Hz to 3 200 Hz. The natural frequencies and mode shapes of the specimens within the specified range are identified.

Finally, the specimen is successfully subjected to pulse vibration through sufficient excitation provided by the combination of a vibration shaker, signal output device, and power amplifier. The excitation amplitude is set to 20 N, and the corresponding time-response curve of the

specimen under this condition is accurately recorded. Furthermore, the sampling frequency is set to 6 400 Hz; the material parameters of the test specimens are summarized in Table 1.

Table 1 Geometrical and material characteristics of the FHCS and DG-FHCS

Type	Parameter
Outside and inside skins	$E_1^{\mathrm{f1,f2}} = 258\,\mathrm{GPa}$, $E_2^{\mathrm{f1,f2}} = 35\,\mathrm{GPa}$, $G_{12}^{\mathrm{f1,f2}} = 3\,\mathrm{GPa}$, $G_{12}^{\mathrm{f1,f2}} = G_{13}^{\mathrm{f1,f2}} = 2\,\mathrm{GPa}$, $\nu_{12}^{\mathrm{f1,f2}} = \nu_{21}^{\mathrm{f1,f2}} = 0.3$, $\rho^{\mathrm{f1,f2}} = 1\,500\,\mathrm{kg/m^3}$, $h_{\mathrm{f1,f2}} = 1\,\mathrm{mm}$, $\kappa_k = [0°/90°/0°]$
Honeycomb core	$E_{\mathrm{h}} = 80\,\mathrm{GPa}$, $\rho_{\mathrm{h}} = 1\,750\,\mathrm{kg/m^3}$, $G_{\mathrm{h}} = 32\,\mathrm{GPa}$, $h^{\mathrm{o}} = 0.008\,\mathrm{m}$, $\theta_{\mathrm{h}} = 60°$, $a = 1 \times 10^{-3}\,\mathrm{m}$, $b = 1 \times 10^{-2}\,\mathrm{m}$
Damping gel	$E_{\mathrm{o}} = G_{\mathrm{o}} = 4.217 \times 10^{-4}\,\mathrm{GPa}$, $\rho_{\mathrm{o}} = 930\,\mathrm{kg/m^3}$
Overall structure	$L = 0.15\,\mathrm{m}$, $R = 0.04\,\mathrm{m}$

4.3 Comparisons of predicted and experimental results

The modal shapes of the structures are presented in the electronic supplementary material. The modal shapes remain similar whether the damping gel is present or absent. Table 2 gives the natural frequencies of the structures. Specifically, the first three modes are selected for comparison: the first mode ($m = 1$, $n = 2$), the second mode ($m = 1$, $n = 1$), and the third mode ($m = 1$, $n = 3$). The results show that the three modal shapes obtained from both methods display a high degree of consistency, with the maximum error in natural frequency being 5.1%. This finding supports the accuracy of the model proposed in Section 2.

Before performing the analysis of transient response behavior, based on the modal test data, the Rayleigh damping parameters for the FHCS ($\xi_1 = 1.98$, $\xi_2 = 2.31$) are determined to be $\eta_1 = 0.004\,79$ and $\eta_2 = 0.003\,83$. For the DG-FHCS ($\xi_1 = 2.79$, $\xi_2 = 6.53$), the corresponding Rayleigh damping parameters are calculated as $\eta_1 = 0.006\,91$ and $\eta_2 = 0.005\,52$.

Table 2 Experimental and theoretical natural frequencies of the FHCS and DG-FHCS

Mode	FHCS		Error/%	DG-FHCS		Error/%
	Experimental frequency/Hz	Theoretical frequency/Hz		Experimental frequency/Hz	Theoretical frequency/Hz	
1st	1 010.0	1 034.8	2.5	989.5	1 014.2	2.5
2nd	1 157.5	1 207.4	4.3	1 134.0	1 183.9	4.4
3rd	1 802.0	1 881.6	4.9	1 765.5	1 855.5	5.1

Using the integration function in the LMS test lab 2021.1 data processing software, the collected acceleration signal is processed using Simpson integration to accurately obtain the displacement signal. When the peak value of different transient excitation loadings is 80 N, the time-response curves derived from both calculation and experimentation are presented in the electronic supplementary material. Tables 3 and 4 give the peak-to-peak values of the vibration responses under different transient excitations. The corresponding maximum error is 6.5%, which falls within the acceptable range for practical engineering applications, thereby validating the effectiveness of the model.

Table 3 Comparison of the test and computational peak-to-peak amplitude without damping gel filled

Type	Rectangular	Triangular	Half-sine	Exponential
Experimental amplitude/m	4.7×10^{-5}	14.2×10^{-6}	23.0×10^{-6}	4.6×10^{-6}
Theoretical amplitude/m	5.0×10^{-5}	15.1×10^{-6}	24.5×10^{-6}	4.9×10^{-6}
Error/%	6.4	6.3	6.5	6.5

Table 4 Comparison of the test and computational peak-to-peak amplitude with damping gel filled

Type	Rectangular	Triangular	Half-sine	Exponential
Experimental amplitude/m	3.1×10^{-5}	12.4×10^{-6}	20.3×10^{-6}	3.3×10^{-6}
Theoretical amplitude/m	3.3×10^{-5}	13.2×10^{-6}	21.6×10^{-6}	3.5×10^{-6}
Error/%	6.4	6.5	6.4	6.1

The primary causes of the prediction error can be attributed to the following factors. (i) The comprehensive account for defects and in-plane residual stresses generated during the manufacturing process of the inner and outer fiber skins are not considered. (ii) The damping effects at the interfaces between the damping glue, honeycomb walls, and inner and outer fiber skins are not taken into account. (iii) The boundary stiffness predicted by the theoretical model is overly idealized, leading to certain numerical inaccuracies. (iv) Young's modulus of the filling honeycomb core layer is simplified and equivalently analyzed using the theoretical model, which to some extent is compromised in terms of the accuracy of the theoretical model. (v) The damping coefficient in the Rayleigh damping model is determined based on parameters such as the natural frequency and damping ratio of the structure, introducing a degree of error.

4.4 Anti-vibration evaluation of the shells with and without damping gel-filled materials

This section presents a comparison of the vibration response between the FHCS and DG-FHCS, and evaluates the vibration-damping performance of the damping gel. The results demonstrate that the damping gel developed and fabricated in this study exhibits effective damping characteristics. A detailed comparative analysis and evaluation of the damping performance are provided in the electronic supplementary material.

5 Influence parameter analysis

In this section, a parametric study is conducted based on the validated model in Section 2. This study explores the influence of several factors on the vibration characteristics of the DG-FHCS structure. These factors include the ratio of honeycomb core thickness to skin thickness, the ratio of honeycomb cell wall thickness to length, and the honeycomb angle. Based on these findings, several important design recommendations are summarized to mitigate the vibration of similar structures. The detailed analysis process is provided in the electronic supplementary material.

6 Conclusions

Through experimental and theoretical investigations, the natural frequency and vibration response of the FHCS and DG-FHCS are analyzed. Detailed solution methodologies are provided, and a convergence analysis along with finite element model validation is conducted. In light of both the theoretical data and experimental findings, the following conclusions can be drawn.

(I) The well-established theoretical model demonstrates high reliability in predicting the natural frequencies and vibration responses of both the FHCS and DG-FHCS. Specifically, the maximum error between the theoretical natural frequency of the FHCS and the experimental results is limited to 4.9%, while for the DG-FHCS, it is confined to 5.1%. Moreover, the maximum discrepancy between the theoretical vibration responses of the FHCS and DG-FHCS and their respective experimental results does not exceed 6.5%.

(II) The established theoretical model can reliably predict the vibration reduction effect of the damping gel. When the excitation is a rectangular wave, the measured and calculated pulse response time attenuation rates are 34.0% and 34.1%, respectively. When the excitation is a

triangular wave, the measured and calculated pulse response time attenuation rates are 12.6% and 12.7%, respectively. When the excitation is a half-sine wave, the measured and calculated pulse response time attenuation rates are 11.8% and 11.7%, respectively. When the excitation is an exponential wave, the measured and calculated pulse response time attenuation rates are 28.6% and 28.3%, respectively, which demonstrates the significant contribution of the damping gel to the dissipation of pulse excitation energy.

(III) This study provides a useful modeling tool for predicting the vibration resistance performance of the DG-FHCS. The modeling, analysis, and manufacturing methods proposed in this study can be easily applied to similar cylindrical shells with filled damping gels, such as composite hydrogen storage shells, composite missile and rocket shells, as well as compression-resistant shells in ocean engineering.

However, material nonlinearity, the bonding effect between layers, and structural vibration problems in thermal environments have not been considered in this study. Therefore, these factors need to be taken into account to develop a more comprehensive modeling methodology for future research. In addition, incorporating multi-material designs or employing machine learning techniques to optimize the structural topology for specific mechanical properties is necessary.

Conflict of interest The authors declare no conflict of interest.

Supporting information Supporting information is available online https://doi.org/10.1007/s10483-025-3304-7.

References

[1] RAMNATH, B. V., ALAGARRAJA, K., and ELANCHEZHIAN, C. Review on sandwich composite and their applications. *Materials Today*: *Proceedings*, **16**, 859–864 (2019)

[2] FU, T., HU, X., and YANG, C. Impact response analysis of stiffened sandwich functionally graded porous materials doubly-curved shell with re-entrant honeycomb auxetic core. *Applied Mathematical Modelling*, **124**, 553–575 (2023)

[3] CHEN, Y. and WANG, Z. W. In-plane elasticity of the re-entrant auxetic hexagonal honeycomb with hollow-circle joint. *Aerospace Science and Technology*, **123**, 107432 (2022)

[4] LI, Z., GAO, Y., WANG, Y., XUE, P., GONG, C., WANG, W., WEI, X., and XIONG, J. Failure mechanisms and acoustic emission pattern recognition of all-CFRP cylindrical honeycomb sandwich shell under three-point bending. *Composites Science and Technology*, **237**, 110003 (2023)

[5] WANG, S., PEI, W., YANG, Y., and DING, Y. Design and analysis of buckling-induced honeycombs with tailorable out-of-plane crushing performance. *Aerospace Science and Technology*, **143**, 108739 (2023)

[6] VASILIEV, V. V., BARYNIN, V. A., and RAZIN, A. F. Anisogrid composite lattice structures — Development and aerospace applications. *Composite Structures*, **94**(3), 1117–1127 (2012)

[7] VASILIEV, V. V. and RAZIN, A. F. Anisogrid composite lattice structures for spacecraft and aircraft applications. *Composite Structures*, **76**(1-2), 182–189 (2006)

[8] XIE, K., CHEN, H., WANG, Y., LI, J., and JIN, F. Nonlinear dynamic analysis of a geometrically imperfect sandwich beam with functionally graded material facets and auxetic honeycomb core in thermal environment. *Aerospace Science and Technology*, **144**, 108794 (2024)

[9] KUMAR, M., KAR, V. R., and CHANDRAVANSHI, M. L. Non-linear vibration and parametric optimization of sandwich composite curved shell panels with graphene reinforced skins and auxetic honeycomb core. *Mechanics Based Design of Structures and Machines*, **52**(8), 5088–5117 (2024)

[10] QUAN, T. Q., ANH, V. M., and DUC, N. D. Natural frequency analysis of sandwich plate with auxetic honeycomb core and CNTRC face sheets using analytical approach and artificial neural network. *Aerospace Science and Technology*, **144**, 108806 (2024)

[11] XU, F., LIU, Z., SELVARAJ, R., and AHSAN, M. Bending and eigenfrequency analysis of glass fiber reinforced honeycomb sandwich shell panels containing graphene-decorated with graphene quantum dots. *Engineering Structures*, **294**, 116685 (2023)

[12] ARUNKUMAR, M. P., PITCHAIMANI, J., and GANGADHARAN, K. V. Bending and free vibration analysis of foam-filled truss core sandwich panel. *Journal of Sandwich Structures & Materials*, **20**(5), 617–638 (2018)

[13] YE, C. and WANG, Y. Q. Nonlinear forced vibration of functionally graded graphene platelet-reinforced metal foam cylindrical shells: internal resonances. *Nonlinear Dynamics*, **104**(3), 2051–2069 (2021)

[14] GUAN, Y. H., ZHAO, D., and LOW, T. S. Experimental evaluation on acoustic impedance and sound absorption performances of porous foams with additives with Helmholtz number. *Aerospace Science and Technology*, **119**, 107120 (2021)

[15] DONG, B., LI, H., LI, K., ZHANG, F., QIAO, Z., YANG, Y., DENG, Y., WANG, S., BAI, H., ZHANG, H., CAO, H., WANG, X., and ZHOU, J. Nonlinear dynamic modeling and experimental study of full-composite cylindrical shells with a foam-filled cavity lattice core. *Nonlinear Dynamics*, **111**(22), 20899–20927 (2023)

[16] LI, Z., LI, H., YANG, Y., DENG, Y., ZHANG, Z., REN, C., WANG, H., ZHOU, B., ZHOU, J., WANG, H., ZHANG, H., LUO, Z., HAN, Q., and GUAN, Z. Nonlinear vibration behaviours of foam-filled honeycomb sandwich cylindrical shells: theoretical and experimental investigations. *Aerospace Science and Technology*, **151**, 109252 (2024)

[17] YANG, J., XIONG, J., MA, L., ZHANG, G., WANG, X., and WU, L. Study on vibration damping of composite sandwich cylindrical shell with pyramidal truss-like cores. *Composite Structures*, **117**, 362–372 (2014)

[18] LI, H., DONG, B., CAO, J., ZHAO, J., XIONG, J., YANG, Y., DU, D., SUN, W., WANG, X., and WU, H. Vibration behaviours of foam-filled grille composite sandwich cylindrical shells. *International Journal of Mechanical Sciences*, **256**, 108533 (2023)

[19] LIU, B. and SUN, Y. Prediction and experiment on the free vibration behavior of carbon-fiber-reinforced cylindrical foldcore sandwich structure. *Composite Structures*, **277**, 114620 (2021)

[20] YADAV, A., AMABILI, M., PANDA, S. K., and DEY, T. Nonlinear analysis of cylindrical sandwich shells with porous core and CNT reinforced face-sheets by higher-order thickness and shear deformation theory. *European Journal of Mechanics-A/Solids*, **90**, 104366 (2021)

[21] VAN QUYEN, N., VAN THANH, T., QUAN, T. Q., and DUC, N. D. Nonlinear forced vibration of sandwich cylindrical panel with negative Poisson's ratio auxetic honeycombs core and CNTRC face sheets. *Thin-Walled Structures*, **162**, 107571 (2021)

[22] LI, H., DONG, B., GAO, Z., ZHAO, J., ZHANG, H., WANG, X., and HAN, Q. Analytical modeling and vibration analysis of fiber reinforced composite hexagon honeycomb sandwich cylindrical-spherical combined shells. *Applied Mathematics and Mechanics* (*English Edition*), **43**(9), 1307–1322 (2022) https://doi.org/10.1007/s10483-022-2858-7

[23] SHAHALI, P., HADDADPOUR, H., and SHAKHESI, S. Dynamic analysis of electrorheological fluid sandwich cylindrical shells with functionally graded face sheets using a semi-analytical approach. *Composite Structures*, **295**, 115715 (2022)

[24] KELESHTERI, M. M. and JELOVICA, J. Analytical solution for vibration and buckling of cylindrical sandwich panels with improved FG metal foam core. *Engineering Structures*, **266**, 114580 (2022)

[25] LIU, Y., ZHU, R., QIN, Z., and CHU, F. A comprehensive study on vibration characteristics of corrugated cylindrical shells with arbitrary boundary conditions. *Engineering Structures*, **269**, 114818 (2022)

[26] LI, H., LIU, D., DONG, B., SUN, K., ZHAO, J., WANG, Q., SUN, W., and WANG, X. Investigation of vibration suppression performance of composite pyramidal truss sandwich cylindrical shell panels with damping coating. *Thin-Walled Structures*, **181**, 109980 (2022)

[27] KARIMIASL, M. and ALIBEIGLOO, A. Nonlinear free and forced vibration analysis of sandwich cylindrical panel with auxetic core and GPLRC facing sheets in hygrothermal environment. *Thin-Walled Structures*, **175**, 109164 (2022)

[28] HEIDARI-SOURESHJANI, A., KALANTARI, A., HESARI, A. E., TALEBITOOTI, R., and TALEBITOOTI, M. Cutout effects on the vibration of sandwich auxetic cylindrical shells with an experimental validation. *Journal of Sound and Vibration*, **592**, 118624 (2024)

[29] JIAN, Z., WANG, Y., ZHAI, J., TANG, C., and GU, Y. Vibration analysis of fiber reinforced composite sandwich cylindrical shells with FG-GPLRPC core under discontinuous boundary conditions. *Structures*, **66**, 106907 (2024)

[30] WU, F., WEI, Y., WU, R., CHEN, X., SHAO, Y., and XUE, X. Dynamic modeling and vibration characteristics of sandwich cylindrical shell with metal-rubber core. *Structures*, **63**, 106305 (2024)

[31] DONG, B., LI, T., ZHANG, L., YU, K., and ZHAO, R. Vibration and response behaviors of composite sandwich cylindrical shells with corrugated-honeycomb blended cores in inhomogeneous thermal environments. *Thin-Walled Structures*, **205**, 112454 (2024)

[32] THANG, P. T., KIM, C., JANG, H., KIM, T., and KIM, J. Free vibration characteristics of honeycomb sandwich cylindrical shells reinforced with graphene nanoplatelets/polymer coatings. *Aerospace Science and Technology*, **156**, 109744 (2025)

[33] YAVARI, F. and ALIBEIGLOO, A. Free vibrations and buckling analyses of sandwich cylindrical shells with auxetic core and shape memory alloy wires reinforced face sheets. *Composite Structures*, **360**, 118994 (2025)

[34] DONG, B., ZHAO, R., and YU, K. Nonlinear vibration of corrugated-honeycomb cylindrical shells in thermal environments. *International Journal of Mechanical Sciences*, **293**, 110200 (2025)

[35] NI, H., LIU, J., LIU, D., CAO, H., and PAN, G. A novel honeycomb sandwich cylindrical shell with dual deformation mode for circumferential vibration isolation and enhanced stiffness. *Mechanical Systems and Signal Processing*, **226**, 112359 (2025)

[36] YADAV, A. Vibration behavior of sandwich circular cylindrical shells with auxetic lattice core and CNT-reinforced facesheets. *Thin-Walled Structures*, **207**, 112716 (2025)

[37] QIN, Z., PANG, X., SAFAEI, B., and CHU, F. Free vibration analysis of rotating functionally graded CNT reinforced composite cylindrical shells with arbitrary boundary conditions. *Composite Structures*, **220**, 847–860 (2019)

[38] ZHU, R., ZHANG, X., ZHANG, S., DAI, Q., QIN, Z., and CHU, F. Modeling and topology optimization of cylindrical shells with partial CLD treatment. *International Journal of Mechanical Sciences*, **220**, 107145 (2022)

[39] GU, X., WANG, L., GUAN, X., WANG, Y., CHENG, Y., and WU, Y. Advances in the design, preparation and application of biomimetic damping materials. *Giant*, **19**, 100321 (2024)

[40] ZHANG, X., ZHANG, X., WANG, P., WANG, X., ZHONG, L., MA, S., and XU, W. Study on viscoelasticity and damping properties of OSA/PAAM hydrogel. *Journal of Polymer Research*, **31**(2), 63 (2024)

[41] DEASTRA, P., WAGG, D. J., SIMS, N. D., and MILLS, R. S. Experimental shake table validation of damping behaviour in inerter-based dampers. *Bulletin of Earthquake Engineering*, **21**(3), 1389–1409 (2023)

[42] KORUK, H. and RAJAGOPAL, S. A comprehensive review on the viscoelastic parameters used for engineering materials, including soft materials, and the relationships between different damping parameters. *Sensors*, **24**(18), 6137 (2024)

[43] ZHANG, C., WANG, Z., ZHU, H., ZHANG, Q., and ZHU, S. Dielectric gels with microphase separation for wide-range and self-damping pressure sensing. *Advanced Materials*, **36**(4), 2308520 (2024)

[44] DING, S. C., FAN, J. F., HE, D. Y., CAI, L. F., ZENG, X. L., REN, L. L., DU, G. P., ZENG, X. L., and SUN, R. High thermal conductivity and remarkable damping composite gels as thermal interface materials for heat dissipation of chip. *Chip*, **1**(2), 100013 (2022)

[45] LI, Z., LI, H., YANG, Y., DENG, Y., ZHANG, Z., REN, C., WANG, H., ZHOU, B., ZHOU, J., WANG, H., ZHANG, H., LUO, Z., HAN, Q., and GUAN, Z. Nonlinear vibration behaviours of foam-filled honeycomb sandwich cylindrical shells: theoretical and experimental investigations. *Aerospace Science and Technology*, **151**, 109252 (2024)

[46] ZHUO, X., XU, P., LI, H., CHU, C., SUN, P., GU, D., SHUAI, S., LI, H., HAN,Q., and WEN, B. C. The analysis of nonlinear vibration characteristics of fiber-reinforced composite thin wall truncated conical shell: theoretical and experimental investigation. *European Journal of Mechanics-A/Solids*, **105**, 105268 (2024)

[47] LI, H., ZHOU, Z., SUN, H., SUN, W., and WEN, B. C. Theoretical study on the influence of hard coating on vibration characteristics of fiber-reinforced composite thin shell. *Coatings*, **8**(3), 87 (2018)

[48] XU, Z., YU, X. C., LI, H., XU, P. Y., SUN, X. C., ZHANG, Y. F., GU, D. W., HAN, Q. K., and WEN, B. C. A mathematical model for analyzing the vibration characteristics of fiber-reinforced thin-walled conical-cylinder composite shells with local bolt missing by the artificial spring method. *Applied Mathematical Modelling*, **136**, 115609 (2024)

[49] XU, Z., YU, X. C., LI, H., XU, P. Y., SUN, X. C., ZHANG, Y. F., GU, D. W., HAN, Q. K., and WEN, B. C. The vibration characteristics analysis of fiber-reinforced thin-walled conical-cylindrical composite shells with artificial spring technique. *International Journal of Structural Stability and Dynamics*, **25**, 2550200 (2025)

[50] LI, H., CAO, J., HAN, J., LI, J., and YANG, Y. Dynamic modeling and vibration suppression evaluation of composite honeycomb hemispherical shell with functional gradient protective coating. *Thin-Walled Structures*, **202**, 112066 (2024)

[51] LI, H., LV, H., GU, J., XIONG, J., HAN, Q., LIU, J., and QIN, Z. Nonlinear vibration characteristics of fibre reinforced composite cylindrical shells in thermal environment. *Mechanical Systems and Signal Processing*, **156**, 107665 (2021)

[52] WANG, C., SONG, X., ZANG, J., and ZHANG, Y. Experimental and theoretical investigation on vibration of laminated composite conical-cylindrical-combining shells with elastic foundation in hygrothermal environment. *Composite Structures*, **323**, 117470 (2023)

[53] DU, D., SUN, W., YAN, X., LIU, H., XU, K., and QIN, Z. Modelling and analysis of nonlinear vibrations for a coupling hard-coated ring disc-cylindric shell structure under piecewise-continuous coupling conditions. *International Journal of Mechanical Sciences*, **215**, 106940 (2022)

[54] LI, J., LI, H., YANG, Y., FANG, Y., WANG, H., WANG, X., ZHANG, H., WANG, H., CAO, H., HOU, J., SUN, G., DU, D., LIU, X., XU, Z., SUN, W., LUO, Z., and HAN, Q. Vibration behaviours of composite conical-cylindrical shells with damping coating: theory and experiment. *Thin-Walled Structures*, **203**, 112218 (2024)

[55] XU, H., WANG, Y., XU, Z., and YU, X. Gegenbauer-Ritz method for free vibration analysis of rotating functionally graded graphene reinforced porous composite stepped cylindrical shells with arbitrary boundary conditions. *Engineering Structures*, **303**, 117555 (2024)

[56] BHRAWY, A. H., TAHA, T. M., and MACHADO, J. A. T. A review of operational matrices and spectral techniques for fractional calculus. *Nonlinear Dynamics*, **81**, 1023–1052 (2015)

[57] LI, J., YANG, Y., HOU, J., WANG, X., ZHANG, H., WANG, H., and LI, H. Vibrational analysis of composite conical-cylindrical shells with functionally graded coatings in thermal environments. *Materials*, **17**(18), 4576 (2024)

[58] LI, H., LIU, D., LI, P., ZHAO, J., HAN, Q., and WANG, Q. A unified vibration modeling and dynamic analysis of FRP-FGPGP cylindrical shells under arbitrary boundary conditions. *Applied Mathematical Modelling*, **97**, 69–80 (2021)

[59] DONG, B., LI, T., ZHANG, L., YU, K., and ZHAO, R. Vibration and response behaviors of composite sandwich cylindrical shells with corrugated-honeycomb blended cores in inhomogeneous thermal environments. *Thin-Walled Structures*, **205**, 112454 (2024)

[60] DONG, B., YU, K., and ZHAO, R. Vibration characteristics and response behaviors of three-dimensional-four-directional knitted composite sandwich cylindrical shells with pyramidal latticed cellular cores. *Composite Structures*, **351**, 118582 (2025)

[61] LI, H., ZOU, Z., LI, J., ZHAO, J., WANG, H., MA, H., and XIE, Z. Nonlinear vibrations of composite cylindrical-cylindrical shells with bolt loosening connection. *International Journal of Structural Stability and Dynamics*, **25**, 2550205 (2025)

[62] WANG, W., GUAN, H., MA, H., WANG, H., MU, Q., ZENG, Y., CHEN, Y., and WEN, B. Dynamic stress analysis of a disc considering actual crack paths: experiment and simulation. *Mechanical Systems and Signal Processing*, **224**, 112199 (2025)

[63] WANG, W., GUAN, H., ZHOU, S., MA, H., and GUO, X. Experimental and numerical study on dynamic behavior evolution of cracked blade-disc. *Mechanical Systems and Signal Processing*, **237**, 113076 (2025)

[64] WANG, W., WU, Z., MA, H., and GUO, X. Through crack effects on the vibration modes of thin discs with elastic support. *Thin-Walled Structures*, **216**, 113661 (2025)

[65] PEETERS, B., VAN DER AUWERAER, H., GUILLAUME, P., and LEURIDAN, J. The PolyMAX frequency-domain method: a new standard for modal parameter estimation? *Shock and Vibration*, **11**(3-4), 523692 (2004)